

# Hybrid Numerical Simulation of Micro Electro Mechanical Systems

M. Greiff, U. B. Bala, and W. Mathis  
University of Hanover, Germany

**Abstract**—In this paper a hybrid numerical approach for the simulation of micro electro mechanical systems (MEMS) is presented. A simulation model that takes into account the mechanical and the electrical effects is developed. The model is applied to an electrostatic force microscope (EFM) and simulation results are presented.

## 1. Introduction

Although micro electro mechanical systems (MEMS) already exist for many applications, their calculation is still difficult since in order to obtain accurate results, often times multi scale aspects have to be included. Furthermore the coupled mechanical and electrical behavior has to be taken into account. In our work this is achieved by dividing the model into a mechanical and an electrical part. The interaction between them is shown in Fig. 1 and can conveniently be realized by using a staggered simulation approach. The electric forces are calculated by the electrical part and passed to the mechanical part which uses them as input for the calculation of the mechanical deflection. In order to apply this approach to a two dimensional model of an electrostatic force microscope (EFM) (Fig. 2) both parts have to be defined. Therefore the components and the principle of an EFM will be explained in the following. An EFM is used to scan surfaces holding an electric potential or a charge distribution [1–3]. During the scanning process the tip at the end of the cantilever is run over the sample. The forces acting on the cantilever and the tip are determined by the electrostatic field and calculated by the electrostatic part of the model. The mechanical behavior of the cantilever is modelled using a beam model while for the region near the tip the finite element method (FEM) is used. A more detailed description of the electrical part will be given in the following.

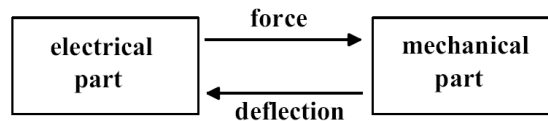


Figure 1: Mechanical and electrical part.

## 2. Formulation of the Problem

The energy-related functional in the electrostatic calculation domain  $\Omega$  (Fig. 2) can be written as

$$W = \int_{\Omega} (\nabla u)^2 d\Omega \quad u \in H_D^1(\Omega) : \{u \in H^1 | u|_{\Gamma_D} = u_0\} \quad (1)$$

where  $u(a_1, a_2, \dots, a_m, x, y)$  is an approximation of the potential  $u(x, y)$ . It is well known that the solution of

$$\frac{\partial W}{\partial a_i} = 2 \int_{\Omega} \nabla u \frac{\partial \nabla u}{\partial a_i} d\Omega = 0 \quad (2)$$

yields an approximative solution for the Laplace equation in  $\Omega$ . In order to solve (2) numerically we shall take a closer look at the requirements in the different parts of the calculation domain  $\Omega$ . Since most of the interaction between probe and sample happens at the bottom of the tip, accurate calculation results are important in this region. Therefore a numerical method which is able to deal with the high field values near the tip is required. For this reason the method of fundamental solutions (MFS) is applied in region  $\Omega_M$  (Fig. 3). At a larger distance from the tip (region  $\Omega_F$ ) lower field values are expected, but possible nonlinearities and charge distributions in the sample require a versatile numerical method such as the finite element method (FEM). Because of the large difference in size of tip and cantilever length, FEM cannot conveniently be applied in the whole rest of the calculation domain. Therefore the boundary element method (BEM) that only requires a mesh on the boundary is used in region  $\Omega_B$ .

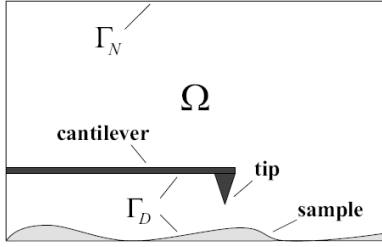


Figure 2: Electrostatic force microscope and calculation domain.

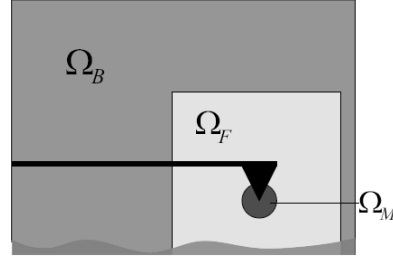


Figure 3: Divided calculation domain.

The solutions in the circular region  $\Omega_M$  of radius  $R$  can be expanded into

$$u(\rho, \phi) = V_0 + \sum_{i=1}^m c_i \left(\frac{\rho}{R}\right)^{\frac{i\pi}{\beta}} \sin\left(\frac{i\pi\phi}{\beta}\right), \quad (\rho, \phi) \in \Omega_M \quad (3)$$

where  $V_0$  is the electric potential and  $\beta$  is the outer opening angle of the tip [4]. For the choice of  $R$  and the position and the number of coupling points, the overlapping area of  $\Omega_M$  and  $\Omega_F$  must be small. Furthermore it must be considered that (3) is a good approximation of the potential only near the tip.

In region  $\Omega_F$  linear FEM

$$u(x, y) = \sum_{j=1}^n u_j \psi_j(x, y), \quad (x, y) \in \Omega_F \quad (4)$$

is applied [5]. The solutions of both regions [6] are coupled by

$$u_c = V_0 + \sum_{i=1}^m c_i \sin\left(\frac{i\pi\phi_c}{\beta}\right). \quad (5)$$

Replacing the coupling node potentials in (4) by (5) and using the resulting potential functions in (2) leads to

$$\begin{pmatrix} M & B^T \\ B & F \end{pmatrix} \begin{pmatrix} c \\ u_F \end{pmatrix} = \begin{pmatrix} b_M \\ b_F \end{pmatrix} \quad (6)$$

where  $\mathbf{M}$  is the matrix resulting from the MFS that is defined by

$$M_{ij} = 2 \sum_{k \in n_c} \sum_{m \in n_c} \sin\left(\frac{i\pi}{\beta} \phi_k\right) \sin\left(\frac{j\pi}{\beta} \phi_m\right) \int_{\Omega_F} \nabla(\psi_k) \nabla(\psi_m) d\Omega + \begin{cases} i\pi, & i = j \\ 0, & \text{otherwise,} \end{cases} \quad (7)$$

$$F_{ij} = 2 \int_{\Omega_F} \nabla\psi_i \nabla\psi_j d\Omega \quad (8)$$

is the FEM stiffness matrix,

$$B_{ij} = 2 \sum_{k \in n_c} \sin\left(\frac{j\pi}{\beta}\right) \int_{\Omega_F} \nabla\psi_i \nabla\psi_k d\Omega \quad (9)$$

is the FEM-MFS coupling matrix,

$$b_{Mi} = -2V_0 \sum_{k \in n_c} \sum_{m \in n_c} \sin\left(\frac{i\pi}{\beta}\right) \int_{\Omega_F} \nabla\psi_k \nabla\psi_m d\Omega \quad (10)$$

is the MFS right hand side and

$$b_{Fi} = -2V_0 \sum_{k \in n_c} \int_{\Omega_F} \nabla\psi_i \nabla\psi_k d\Omega - 2 \sum_{j \in n_D} \phi_j \int_{\Omega_F} \nabla\psi_i \nabla\psi_j d\Omega \quad (11)$$

is the right hand side resulting from the variation of the FEM potentials. Here  $n_c$  stands for the coupling nodes and  $n_D$  are the Dirichlet boundary conditions. The matrix  $F$  can be written as

$$\mathbf{F} = \begin{pmatrix} F_{NN} & F_{CN}^T \\ F_{CN} & F_{CC} \end{pmatrix} \quad (12)$$

where  $F_{NN}$  includes only the interaction between the nodes inside the FEM domain,  $F_{CC}$  stands for the interaction inside the coupling interface while the interaction of coupling interface and FEM domain is described by  $F_{CN}$ .

On the FEM-BEM transmission interface  $\Gamma_T = \Gamma_B \cap \Gamma_F$ :  $u_B = u_F$  and  $\frac{\partial u_B}{\partial n} + \frac{\partial u_F}{\partial n} = 0$ . Using the Gauss theorem on  $\Omega_{FM} = \Omega_F \cup \Omega_M$  one obtains [5]

$$\int_{\Gamma_F} \frac{\partial u_{FM}}{\partial n} v \, d\Gamma = \int_{\Omega_{FM}} \operatorname{div}(\nabla u_{FM} \cdot v) \, d\Omega = \int_{\Omega_{FM}} \Delta u_{FM} \cdot v \, d\Omega + \int_{\Omega_{FM}} \nabla u_{FM} \cdot \nabla v \, d\Omega \quad (13)$$

i. e., for all  $v \in H_{D,0}^1(\Omega_{FM}) := \{v \in H^1(\Omega_{FM}) : v|_{\Gamma_D \cap \Gamma_F} = 0\}$

$$a(u_{FM}, v) := \int_{\Omega_{FM}} \nabla u_{FM} \cdot \nabla v \, d\Omega = \int_{\Omega_{FM}} f \cdot v \, d\Omega + \int_{\Gamma_F} \frac{\partial u_{FM}}{\partial n} v \, d\Gamma =: (f, v)_{\Omega_{FM}} + \left\langle \frac{\partial u_{FM}}{\partial n}, v \right\rangle_{\Gamma_F} \quad (14)$$

where  $u_{FM}$  includes  $u_F$  and  $c$ . The representation formula of the Laplace equation for the solution of  $u_B$  inside  $\Omega_B$

$$u_B(x) = \int_{\Gamma_B} \left\{ \frac{\partial}{\partial n(y)} G(x, y) u_B(y) - G(x, y) \frac{\partial u_B}{\partial n(y)} \right\} d\Gamma, \quad x \in \Omega_B \quad (15)$$

with the fundamental solution of the Laplacian given by

$$G(x, y) = -\frac{1}{2\pi} \log |x - y|. \quad (16)$$

If one computes the Cauchy data [7]  $u_B$  and  $\partial u_B / \partial n$  of  $u_B(x)$ , one will get two boundary integral equations on  $\partial\Omega_B$ ,

$$V \frac{\partial u_B}{\partial n} = (I + K) u_B \quad (17)$$

$$W u_B = (I - K') \frac{\partial u_B}{\partial n} \quad (18)$$

where the boundary integral operators are defined as

$$V\psi(x) := 2 \int_{\Gamma_B} G(x, y) \psi(y) d\Gamma_y, \quad K\psi(x) := 2 \int_{\Gamma_B} \frac{\partial}{\partial n_y} G(x, y) \psi(y) d\Gamma_y, \quad x \in \Gamma_B \quad (19)$$

$$K'\psi(x) := 2 \frac{\partial}{\partial n_x} \int_{\Gamma_B} G(x, y) \psi(y) d\Gamma_y, \quad W\psi(x) := -2 \frac{\partial}{\partial n_x} \int_{\Gamma_B} \frac{\partial}{\partial n_y} G(x, y) \psi(y) d\Gamma_y, \quad x \in \Gamma_B \quad (20)$$

where the single layer potential  $V$  and the hypersingular operator  $W$  are symmetric and the double layer potential  $K$  has the dual  $K'$  [8].

Using (18) one can eliminate  $\partial u_B / \partial n$  with (17). This leads to

$$W u_B = (I - K') \frac{\partial u_B}{\partial n} = 2 \frac{\partial u_B}{\partial n} - (I + K') \frac{\partial u_B}{\partial n} = 2 \frac{\partial u_B}{\partial n} - (I + K') V^{-1} (I + K) u_B \quad (21)$$

with the Poincaré-Steklov-Operator  $S$  applied to  $u_B$

$$S u_B := (W + (I + K') V^{-1} (I + K)) u_B = 2 \frac{\partial u_B}{\partial n} \quad (22)$$

which can be used for symmetric coupling. In variational form for all  $w \in \tilde{H}^{1/2} := \{w \in H^{1/2}(\Gamma_B) : w|_{\Gamma_D \cap \Gamma_B} = 0\}$  holds

$$\langle S u_B, w \rangle_{\Gamma_B} = 2 \left\langle \frac{\partial u_B}{\partial n}, w \right\rangle_{\Gamma_B}. \quad (23)$$

With (14) and (23) one can obtain the variational formulation

$$2a(u_{FM}, v) + \langle S u_B, v \rangle_{\Gamma_T} = 2(f, v)_{\Omega_{FM}} + 2\langle t_0, v \rangle_{\Gamma_N \cap \Gamma_F} \quad (24)$$

$$\langle S u_B, w \rangle_{\Gamma_B \cap \Gamma_N} = 2\langle t_0, w \rangle \quad (25)$$

for all  $(w, v) \in \tilde{H}^{1/2} \times H_{D,0}^1(\Omega_F)$  with  $f$  being the charge distribution inside  $\Omega_F$  and  $t_0$  are the Neumann boundary conditions.

The Poincaré-Steklov-Operator  $S$  cannot discretize directly because the inverse single layer potential  $V$  cannot be discretized in the usual way. For this reason without Poincaré-Steklov-Operator the problem can be rewritten as saddle point formulation. The saddle point formulation of the problem for all  $(w, v, \psi) \in \tilde{H}^{1/2} \times H_{D,0}^1(\Omega_{FM}) \times \tilde{H}^{-1/2}(\Gamma_B)$

$$2a(u_{FM}, v) + \langle Wu_B, v \rangle_{\Gamma_T} + \langle (I + K')\varphi, v \rangle_{\Gamma_T} = 2(f, v)_{\Omega_{FM}} + 2\langle t_0, v \rangle_{\Gamma_N \cap \Gamma_F} \quad (26)$$

$$\langle Wu_B, w \rangle_{\Gamma_B \cap \Gamma_N} + \langle (I + K')\varphi, w \rangle_{\Gamma_B \cap \Gamma_N} = 2\langle t_0, w \rangle_{\Gamma_B \cap \Gamma_N} \quad (27)$$

$$\langle (I + K)u_B, \psi \rangle_{\Gamma_B} - \langle V\varphi, \psi \rangle_{\Gamma_B} = 0 \quad (28)$$

If the bases are introduced as  $\text{span}\{v_1, \dots, v_F\} = X_F$ ,  $\text{span}\{w_1, \dots, w_B\} = X_B$  and  $\text{span}\{\psi_1, \dots, \psi_F\} = Y_B$ , the basis functions of  $X_F$  and  $X_B$  are supposed to be ordered such that

$$\text{span}\{v_1, \dots, v_F\} = X_F \cap H_{D,0}^1(\Omega_F)$$

$$\text{span}\{w_1, \dots, w_B\} = X_B \cap H^{1/2}(\Gamma_B).$$

If the coefficients of  $u_{FM}$  and  $u_B$  are denoted by  $u$  and the coefficients of  $\varphi$  are denoted by  $\varphi$  again then this system is equivalent to the original differential equation that can be used for discretization. This system corresponds to a matrix formulation which can be written as

$$\begin{pmatrix} M & B^T & 0 & 0 & 0 \\ B & F_{NN} & F_{NC} & 0 & 0 \\ 0 & F_{CN} & F_{CC} + W_{CC} & W_{CN} & (K^T + I)_C \\ 0 & 0 & W_{NC} & W_{NN} & (K^T + I)_N \\ 0 & 0 & (K + I)_C & (K + I)_N & -V \end{pmatrix} \begin{pmatrix} u_m \\ u_F \\ u_T \\ u_B \\ \varphi \end{pmatrix} = \begin{pmatrix} b_m \\ b_F \\ b_\Gamma \\ b_B \\ b_\varphi \end{pmatrix} \quad (29)$$

where the subscript  $C$  means contribution from the coupling nodes and  $N$  means contribution from the noncoupling nodes. Finally the blocks  $W$ ,  $V$ ,  $K + I$ , and  $K^T + I$  provide the coupling between the two ansatz spaces  $X_F$  and  $X_B$ . Here  $u_m$  are the MFS coefficients,  $u_F$  and  $u_B$  are the nodal potentials inside the FE domain and on the boundary of the BE domain respectively,  $u_T$  are the nodal potentials on the FE-BE coupling interface and  $\varphi$  are the normal components of the electric field distribution on the boundary of the BE domain. The vector  $b$  includes the corresponding boundary conditions. As the matrix in (29) is not positive definite, a specific algorithm such as the MINRES algorithm is required for the solution.

Since the scanning process of an EFM is dynamic, the FEM mesh in  $\Omega_F$  has to be changed during the calculation which is achieved by using the arbitrary Lagrangian Eulerian method (ALE) [9]. The mesh is modeled as a massless elastic which is deformed by the changing position of the cantilever and the sample (Fig. 4).

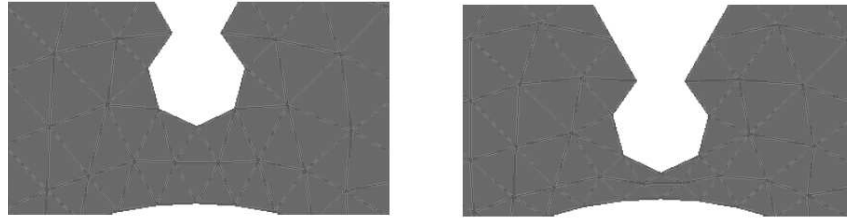


Figure 4: ALE mesh deformation.

The result of a typical simulation can be seen in Fig. 6 and Fig. 7. As expected a high value of the electric field occurs at the tip. Since the coupling condition of MFS and FEM only includes the potential values (5), the electric field is not continuous on the interface. This indicates that FEM simulation results near the tip can be improved by using the coupled FEM-MFS approach presented here. A smoother transition of the electric field can be obtained by using a combination of FEM and MFS ansatz functions in region  $\Omega_M$ . Fig. 5 shows the simulated potential between tip and sample obtained by using FEM and the hybrid simulation approach ( $R = 1, 2$ ).

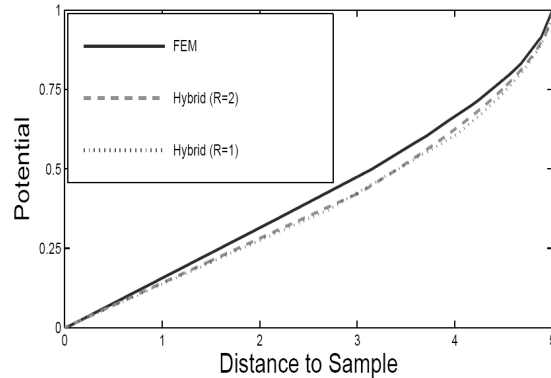


Figure 5: Comparison FEM/Hybrid Simulation.

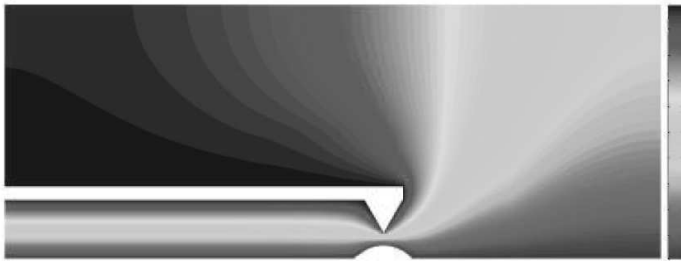


Figure 6: Simulated electrostatic potential.

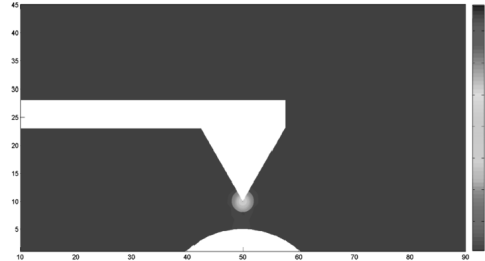


Figure 7: Simulated electrostatic field.

### 3. Conclusion

A hybrid numerical approach for the simulation of micro electro mechanical systems (MEMS) has been presented and applied to an electrostatic force microscope. In order to fulfill the special requirements in the different simulation regions an approach that combines FEM BEM and MFS was used to calculate the electrostatic field. ALE was applied to fit the FEM mesh to the changing boundaries. The results show the expected field distribution.

### Acknowledgment

The authors would like to thank T. Helmich and Prof. Dr.-Ing. U. Nackenhorst (Institute of Mechanics and Computational Mechanics, Hanover University) for their contribution in the implementation of the mechanical model. We also thank PD Dr. rer. nat. M. Maischak (Institute of Applied Mathematics, Hanover University) for his contribution and valuable discussions on numerical coupling. This work has been supported by the German Research Foundation (DFG), GRK 615.

### REFERENCES

1. Bhushan, B., *Handbook of Nano-technology*, Springer, Berlin, 2004.
2. Morita, S., R. Wiesendanger, and E. Meyer, *Noncontact Atomic Force Microscopy*, Springer, 2002.
3. Jacobs, H. O., P. Leuchtman, O. J. Homan, and A. Stemmer, "Resolution and contrast in Kelvin probe force microscopy," *Journal of Applied Physics*, Vol. 84, No. 3, 1998.
4. Jackson, J. D., *Classical Electrodynamics*, Wiley, 1975.
5. Reddy, J. N., *Finite Element Method*, McGraw-Hill International Editions, Singapore, 1993.
6. Li, Z. C., *Numerical Methods for Elliptic Problems with Singularities*, World Scientific, 1990.
7. Costabel, M., "A symmetric method for the coupling of finite elements and boundary elements," *The Mathematics of Finite Elements and Applications*, Vol. 6, 281–288, 1988.
8. Stephan, E. P., "Coupling of boundary element methods and finite element methods," *Encyclopedia of Computational Mechanics*, Vol. 1, Chapter 13, 375–412, 2004.
9. Belytschko, T., W. K. Liu, and B. Moran, *Nonlinear Finite Elements for Continua and Structures*, Wiley, Sussex, 2004.